

# Effect of Current Density on Electrodeposited Ni-TiC-WC Composite Coating and Evaluating the Corrosion Resistance of the Coating and Substrate in NaCl Solution

Ali Keramatian<sup>1</sup>, Mohammad Hossein Enayati<sup>1</sup>, Fatemeh Sadat Sayyedani<sup>2,\*</sup>, Sima Torkian<sup>1</sup>

\* sayyedani@um.ac.ir

<sup>1</sup> Department of Materials Engineering, Isfahan University of Technology, Isfahan 8415683111, Iran

<sup>2</sup> Department of Materials Science and Engineering, Faculty of Engineering, Ferdowsi University of Mashhad, Mashhad 9177948944, Iran

Received: November 2024

Revised: April 2025

Accepted: May 2025

DOI: 10.22068/ijmse.3839

**Abstract:** This study aimed to investigate the effect of current density on the microstructure of electrodeposited Ni-WC-TiC composite coatings on 304 stainless steel and compare the corrosion resistance of the coating and substrate in a 3.5 wt.% sodium chloride solution. A Watts nickel bath was employed under direct current (DC) conditions. Microstructure, elemental composition, and phase composition analyses were conducted using scanning electron microscopy (SEM) equipped with energy-dispersive X-ray spectroscopy (EDS) and X-ray diffraction (XRD), respectively. The results revealed that the coating formed at a current density of 40 mA/cm<sup>2</sup> exhibited a denser microstructure with higher cohesion and uniformity than coatings produced at other current densities. The corrosion resistance of the coating and substrate was evaluated using Tafel and electrochemical impedance spectroscopy (EIS) analyses. The corrosion test results indicated that the substrate exhibited superior corrosion resistance compared to the coating. Based on the dynamic polarization test plots, the corrosion mechanism of the substrate is active-quasi passive, with a pseudo-passive layer forming on the sample, which remains stable within the potential range of -0.17 to 0.17 V. Beyond this likely range, the sample becomes susceptible to pitting. In the coated sample, the corrosion behavior is similar to that of the substrate, except that the pseudo-passive layer remains stable within a narrower potential range of -0.19 to 0.08 V.

**Keywords:** Electrodeposition, Ni-WC-TiC, Composite coating, Corrosion resistance.

## 1. INTRODUCTION

Surface protective coatings are highly in demand to improve materials' corrosion resistance by extending the parts' lifetime [1, 2]. Employing composite structures to enrich the properties and performance of the coating has been of great interest in recent years [11, 2-5]. The performance of the coatings can be improved by embedding reinforcing ceramic particles such as oxides (Al<sub>2</sub>O<sub>3</sub>), nitrides (TiN), carbides (WC, TiC), and intermetallic compounds (NiAl) within the composite matrix [2-5]. While the composite matrix could be Ni, Fe, Cu, Co, etc., nickel-based composite coatings are more in demand due to their desired mechanical properties and low cost [5, 6]. Nickel coatings are widely used in petrochemical, textile [1], aerospace, piston rings, cylinders [3] and catalyst (Ni-CeO<sub>2</sub> composite) [7]. Corrosion is an aggressive phenomenon with economic and equipment losses, which can be moderated by employing composite coatings [2]. The observations have demonstrated that the corrosion resistance of nickel composite coatings

is better than that of the pure nickel coating, due to the formation of the oxide layer and ceramic particles on the surface [8]. Adding tungsten to the matrix can improve the corrosion properties of nickel-based coatings [3, 8, 9]. Surender et al [4] investigated the corrosion resistance of electrodeposited Ni-WC composite coating. They realised that the Ni-WC composite had higher current density and passive potential than pure nickel. Adding Tin to the Ni-W composite by the pulse electrodeposition method, Zhang et al [2] investigated the corrosion resistance of the composite coating and reported an improvement in the corrosion behaviour of the composite coating in the presence of Tin.

While many methods exist to produce composites, the electrodeposition method could be one of the best processes [10, 12]. Electrodeposition has been favoured due to its ability to create complex shapes, low cost, reproducibility, and waste reduction [1, 10].

This study aimed to investigate the effect of current density on the microstructure of electrodeposited (Ni-WC-TiC) composite coatings on AISI 304

stainless steel substrates, using micrometer-sized ceramic particles. After achieving optimal coating adhesion at the determined current density, the coating and substrate's corrosion resistance were evaluated in a 3.5 wt.% sodium chloride (NaCl) solution.

## 2. EXPERIMENTAL PROCEDURES

AISI 304 stainless steel was cut into  $2 \times 2 \text{ cm}^2$  coupons. A copper wire was connected to the pieces to conduct an electric current. The samples were mounted and ground using 80 to 1200 SiC grit paper. The substrates were degreased in an ultrasonic bath, subjected to acetone and distilled water for 20 minutes, respectively. Finally, the samples were subjected to the pre-electrodeposition process according to Table 1 to achieve better adhesion strength between the coating and the substrate.

**Table 1.** The solutions used in the surface preparation stage for the subsequent composite electroplating

Process No.	Solution	Time (s)	Details
1	6 ml distilled water + 4 ml HCl	50	Surface Activation
2	30 ml distilled water + 70 ml $\text{H}_2\text{SO}_4$	180	Current density= 107 $\text{mA}/\text{cm}^2$ - Anodic electrodeposition
3	120 ml HCl + 240 g/l NiCl	120	Current density= 108 $\text{mA}/\text{cm}^2$ - Cathodic electrodeposition

To activate the surface of the substrate, the mounted coupons were immersed in the first solution. In the second solution, the piece was used as an anode, due to the detachment of atoms from the surface and roughening the substrate surface. The coupons were connected to the cathode in the third solution to deposit NiCl on the 304 stainless steel surface. In the third stage, the carbide particles acquire a positive charge due to the applied electric field and migrate toward the cathode (substrate). Simultaneously, nickel ions undergo reduction by electron uptake and deposit onto the substrate, entrapping the ceramic particles within the growing metallic matrix [29]. Watts bath was prepared according to Table 2 with a volume of 200 ml and let rest for 24 h. To prevent carbide particles from settling, the prepared solution was placed in an ultrasonic bath for 15

min immediately before the start of the plating process. The carbide particles had a size of less than  $25 \text{ }\mu\text{m}$ , with a TiC/WC ratio of 1:2. The pH of the solution was adjusted by  $\text{NH}_3$  and 98 vol.% diluted sulfuric acid using a digital PH meter (Metrohm, Switzerland) within the specified range. The electrodeposition process was run using the direct current method and a digital coulometer device (Behpajooh, Iran) under a temperature of  $50^\circ\text{C}$ , and the conditions are presented in Table 3. The samples were rinsed with ethanol after the coating process. This research used electrodeposition under four different current densities of 30, 35, 40, and  $50 \text{ mA}/\text{cm}^2$ . Fig. 1 depicts an overview of the Watts solution and the presence of WC and TiC particles for the coating process.

**Table 2.** Watts bath composition for nickel electrodeposition

Composition	Concentration (g/l)	Company
$\text{NiCl}_2 \cdot 6\text{H}_2\text{O}$	45	MERCK
$\text{H}_3\text{BO}_3$	40	MERCK
TiC-WC	6	MERCK
$\text{NiSO}_4$	250	MERCK

**Table 3.** Nickel electrodeposition conditions

Current	DC
Temperature ( $^\circ\text{C}$ )	$50 \pm 2$
pH	$4.4 \pm 0.1$
Colon (A.S)	27
Anode	Nickel
Cathode	AISI 304 stainless steel

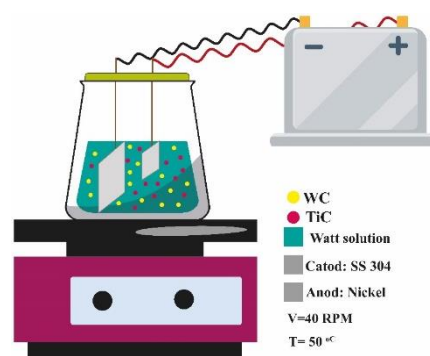


**Fig. 1.** Schematic of the Watts solution used in the coating process

The surface morphology of the coatings was observed using a scanning electron microscope (SEM, Philips XL30). The elemental composition of the produced composite was analyzed by energy dispersive spectroscopy (EDS). The phase

composition of the coatings was investigated by X-ray diffraction (XRD) method (40 Kv, Cu K $\alpha$ ). Phase analysis was performed using X'Pert HighScore software. The coating's crystallite size (d) was determined using the Scherrer equation (Eq. 1).

$$d = K\lambda / \beta \cos\theta \quad (1)$$

Where k is the Scherrer's constant with the value of 0.91,  $\lambda$  is the wavelength of the beam used (1.542 Å for copper),  $\beta$  is the peak width at half-height (FWHM), and  $\theta$  is the Bragg diffraction angle. Electrochemistry Impedance spectroscopy (EIS) and Potentiodynamic polarization tests were performed in 3.5 wt% NaCl solution to examine the corrosion behavior of the coated and uncoated samples.

The three-electrode electrochemical cell, consisting of the sample as the working electrode, a KCl saturated Ag/AgCl electrode as the reference electrode, and a platinum electrode as the counter electrode, was connected to the potentiostat device

(Ivium, Netherlands). After immersing the sample in a 3.5 wt.% NaCl electrolyte for one hour, the Electrochemical Impedance Spectroscopy (EIS) test was conducted within the frequency range of 100 kHz to 10 mHz at a voltage amplitude of 10 mV followed by the dynamic polarization test in the potential range from -250 mV relative to the open-circuit potential (OCP) to 1.6 V relative to the reference electrode. The surface morphology of the samples after the corrosion test in a salt environment was observed by scanning electron microscope (SEM, Philips XL30).

### 3. RESULTS AND DISCUSSION

The SEM micrographs of the coatings with current densities of 30, 35, 40, and 50 mA/cm<sup>2</sup> and carbide concentration of 6 g/l are presented in Fig. 2. It can be seen that a uniform and dense coating could be achieved by increasing the current density up to 40 mA/cm<sup>2</sup>.



**Fig. 2.** SEM micrographs of Ni–WC–TiC composite coating surface at different current densities: a) 30 mA/cm<sup>2</sup>, b) 35 mA/cm<sup>2</sup>, c) 40 mA/cm<sup>2</sup>, d) 50 mA/cm<sup>2</sup>



Further increase in current density up to 50 mA/cm<sup>2</sup> caused a decrease in the uniformity and density of the coating, with some scattered carbide particles deposited in the matrix. It is known that for a constant carbide concentration, the growth rate of the nuclei remains almost the same with the reduction of the current density, and a more uniform morphology would be obtained [13]. At lower current densities, the deposits on the cathode surface are limited [14, 15]. At the optimal current density (40 mA/cm<sup>2</sup>), the growth of nickel is sufficient to trap deposits in a specific period of time, leading to an increase in deposition. On the other hand, the rate of carbide deposition increases with increasing current density, followed by an increase in the growth rate of the coating and the amount of carbide deposited [14, 16, 17]. Therefore, it will be possible to choose the optimal limit of the current density to achieve a uniform and dense coating, based on the observations of surface morphology and elemental analysis.

Fig. 3 represents the EDS analysis of the coating at different current densities. Accordingly, as the current density increases, the percentage of carbide deposition increases, which can be explained by the Faraday's first law (Eq. 2) [17]:

$$m = Kq = Kit \quad (2)$$

Where *m* is the mass deposited, *I* is the electrical current, *t* is the electrolysis time, *q* is the total charge, and *K* is the equivalent weight of the electrolyte. The equivalent weight is expressed

as atomic weight divided by valency. According to equation (2), *m* is proportional to *I*. It means that the higher the current density, the more ions carrying the composite agent in the solution followed by an increase in the deposited mass. The results of the EDS analysis of the coating at different current densities also confirmed this fact (Fig. 3).

According to the SEM images and EDS analysis of the coating in different current densities, the current density of 40 mA/cm<sup>2</sup> was obtained to be the optimal current density in which a uniform and dense coating with desired amount of double carbide deposition would be obtained. In the next section, the results of the XRD analysis and corrosion resistance of the coating will be discussed at the optimal current density of 40 mA/cm<sup>2</sup>.

Fig. 4 illustrates the cross-sectional morphology of the coating at a current density of 40 mA/cm<sup>2</sup>. As observed, the coating is densely packed and fully adhered to the substrate surface, with a thickness ranging from 10 to 37 μm. However, at greater coating thicknesses, the uniformity diminishes, and the coating tends to accumulate in localized areas. This discontinuity and non-uniformity could also be attributed to the cutting process performed on the sample to observe the cross-section. On average, the coating thickness was measured to be 24±0.8 μm. The dark areas in Fig. 3 represent nickel particles as the matrix, while the white areas indicate undissolved WC particles within the composite matrix.



**Fig. 3.** EDS analysis of Ni–WC–TiC composite coating at different current densities: a) 30 mA/cm<sup>2</sup>, b) 35 mA/cm<sup>2</sup>, c) 40 mA/cm<sup>2</sup>, and d) 50 mA/cm<sup>2</sup>

The WC particles have retained their structure and accumulated at the end of the coating. Due to the addition of Ti to the coating, the number of these particles is not significant. Ti facilitates the dissolution of WC particles in the coating [18].



**Fig. 4.** SE-SEM image of the cross section of the Ni-WC-TiC composite coating at the current density of 40 mA/cm<sup>2</sup>

The XRD analysis of the coating at the current density of 40 mA/cm<sup>2</sup> is presented in Fig. 5. The obtained diffraction patterns indicated the presence of the Ni phase with a cubic crystal structure and ceramic hard phases of WC-TiC in the composite coating. X'pert High Score software calculates the crystallite size using equation 1. The calculated crystallite size for the index peak according to the Scherrer equation was obtained to be 390 Å. The EIS test plots are presented in Fig. 6, including Nyquist, Term, and Bode phase diagrams. The data extracted from the ZView software are summarized in Table 4 and the equivalent circuit corresponding to the impedance curves is shown in Fig. 7. In the Nyquist plot, a larger loop radius indicates higher resistance of the sample [27]. According to Fig. 6a, the substrate exhibits greater resistance compared to the coated sample. Additionally, the Term and Bode phase plots reveal the presence of

three time constants, indicating three loops in the equivalent circuit predicted by ZView software. The presence of three distinct regions with varying slopes and concavities suggests the existence of three time constants and, consequently, three loops in the equivalent circuit. The three-loop configuration of the equivalent circuit can be attributed to the corrosion phenomenon, which introduces three time constants:  $R_s$ , representing the solution resistance;  $R_1$ , representing the resistance of the passive layer;  $R_2$ , corresponding to the charge transfer resistance of the steel sample's dissolution process within pits; and  $R_3$ , representing charge transfer resistance. A constant phase element (CPE) is also employed to account for the non-ideal capacitance due to the deviation of the semicircle from a perfect circular shape [26].



**Fig. 5.** XRD analysis of the Ni-WC-TiC composite coating at the current density of 40 mA/cm<sup>2</sup>

The impedance of CPE is defined as below [20]:

$$Z_{CPE} = \frac{1}{Q(\omega.i)^{-n}} \quad (3)$$

Where  $Q$  and  $n$  (between 0-1) are constants of CPE,  $\omega$  is angular frequency, and  $i$  is an imaginary number ( $i^2 = -1$ ).

As can be observed from the plots and the results presented in Table 4, the substrate sample exhibits higher corrosion resistance compared to the coated one.

The results of the potentiodynamic polarization test in 3.5 wt.% NaCl solution for the coated and uncoated samples is presented in Fig. 8. The results extracted from the polarization plots (Fig. 8) are presented in Table 5, where " $E_b$ " and " $E_{corr}$ " represent the breakdown potential of the passive layer and the corrosion potential of the samples, respectively.



Fig. 6. The curves obtained from the impedance test: a) Nyquist, b) Term phase, and c) Bode phase

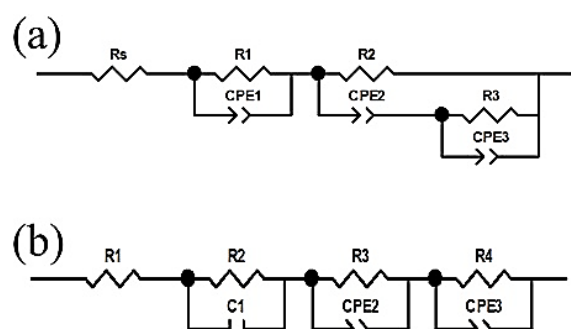


Fig. 7. The equivalent circuit predicted by the ZView software including the equivalent circuit of a) the coating b) the substrate

Table 4. The parameters extracted from the impedance test results by Z-View software

Parameter	Substrate	Coating
$R_s (\Omega.cm^2)$	20	46.57
$R_1 (\Omega.cm^2)$	2077	581.7
$Q_1 (F/cm^2)$	-	$10.8 \times 10^{-5}$
$n_1$	-	0.91
$R_2 (\Omega.cm^2)$	47.86	63370
$Q_2 (F/cm^2)$	$2.2 \times 10^{-7}$	$20.1 \times 10^{-5}$
$n_2$	0.96	0.83
$R_3 (\Omega.cm^2)$	600480	17556
$Q_3 (F/cm^2)$	$0.36 \times 10^{-4}$	$8.6 \times 10^{-5}$
$n_3$	0.78	0.81
$C_1 (F/cm^2)$	$308.8 \times 10^{-6}$	-
Chi-squared	0.0013	0.0003

Based on the dynamic polarization test plots, the corrosion mechanism of the substrate is active-quasi passive, with a pseudo-passive layer forming on the sample which remains stable within the potential range of -0.17 to 0.17 V. Beyond this potential range, the sample becomes susceptible to pitting. In the coated sample, the corrosion behavior is similar to that of the substrate, except that the pseudo-passive layer remains stable within a narrower potential range of -0.19 to 0.08 V. According to the corrosion theories, the corrosion intensity depends on the number and size of holes

and defects present in the coating. The holes in the coating cause the formation of micro galvanic cells by transferring the electrolyte from the environment to the coating/substrate interface leading to an increase in the corrosion rate [19]. Also, coating defects such as porosity, coating layer thickness, and microcracks affect the corrosion resistance. These defects cause chloride ions to reach the substrate and increase susceptibility to pitting corrosion [21, 28].

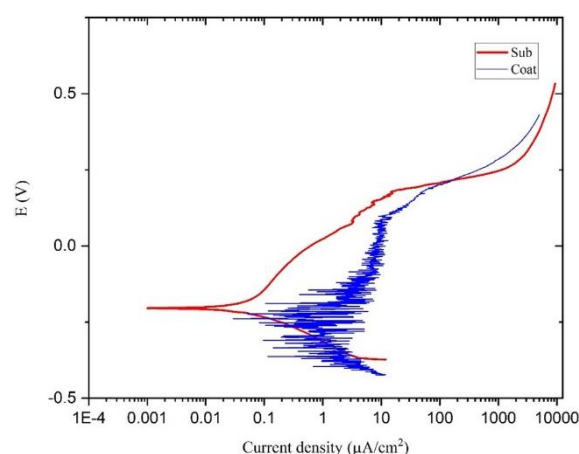


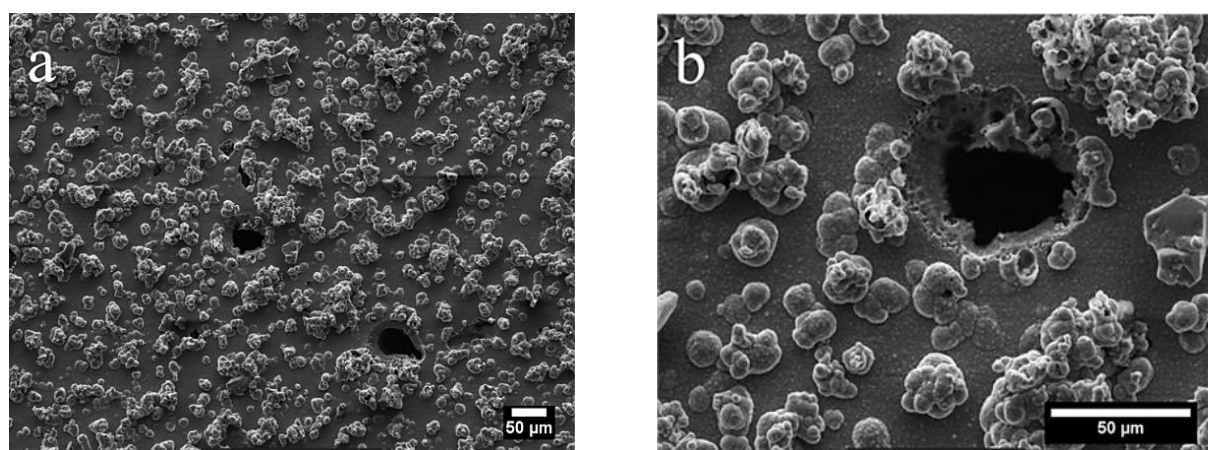
Fig. 8. Polarization test of the coated and uncoated samples in 3.5 wt.% NaCl solution

Table 5. The results of the polarization test for the substrate and coating

Sample	$E_{corr} (V)$	$E_b$
Substrate	-0.22	0.17
Composite coating	-0.29	0.08

Fig. 9 presents the SEM images of the surface of the coated sample at the current density of 40 mA/cm<sup>2</sup> after corrosion in 3.5 wt.% NaCl solution with two different magnifications. The composite coating has some small and large holes responsible for chloride ion transport to the substrate's surface, causing pitting and galvanic corrosion of the coating and the substrate.





**Fig. 9.** SEM images of the surface of the coated sample with a current density of 40 mA/cm<sup>2</sup> after corrosion in 3.5 wt.% NaCl solution with two different magnifications

Another reason for pitting and galvanic corrosion is the presence of nickel. The corrosion mechanism of Ni coating is mainly pitting and galvanic corrosion [22]. Xia et al [23] reported that small-sized ceramic particles can significantly increase the corrosion resistance and stability of the metal-matrix composites. So, the small particles of TiC and WC in the Ni matrix can provide the best corrosion resistance for the coating. As a result, with the presence of WC particles in the composite coating, Ni matrix is less exposed to corrosion and the corrosion resistance of the coating increases. This effect is also observed in the presence of grain boundaries that have low corrosion resistance. So, the corrosion resistance of the coating increases in the presence of WC in the grain boundaries [22, 24, 25]. Fig. 9 reveals that due to the creation of macro and micro particles and the creation of small and large holes during deposition of the coating, the homogeneous structure of the coating has been partially destroyed, leading to the transfer of electrolyte from minor defects to the substrate. This issue causes a small change in the corrosion resistance of the substrate. Not much change in the corrosion resistance of the coating compared to the substrate is due to the non-uniform distribution of WC and TiC carbide particles in the nickel matrix. Another reason could be the low amount of WC and TiC carbides in the Watts bath solution. In this case, the pitting corrosion mechanism in nickel (the main corrosion mechanism) is activated, and the corrosion phenomenon starts for the coating. But, in the case of a more uniform distribution of carbide particles or a larger number of carbides, the corrosion resistance increases as the presence

of the carbide particles increases the corrosion resistance of the coating.

#### 4. CONCLUSIONS

In this research, Ni–WC–TiC composite coating was applied on the AISI 304 stainless steel by the electrodeposition method and the effect of current density on the coating microstructure was investigated at the constant carbide concentration of 6 g/l. The results of the SEM/EDS observations revealed that the optimal current density to achieve a denser microstructure with more continuity and uniformity compared to others was 40 mA/cm<sup>2</sup>. The impedance and polarization tests of the substrate and coating revealed the greater resistance of the substrate compared to the coating, as well as the quasi-passive behavior of the samples in the polarization test.

#### REFERENCES

- [1] S. Khorsand, M. Karbasi, F. S. Sayyedan, M. Eshaghian, and M. Razavi, Development of electroco-deposited Ni–Fe(Ti,W)C nanocomposite coatings, *Surf. Eng.* 34 (2018) 433–439. doi:10.1080/02670844.2017.1370880.
- [2] W. Zhang, B. Li, and C. Ji, Synthesis and characterization of Ni–W/TiN nanocomposite coating with enhanced wear and corrosion resistance deposited by pulse electrodeposition, *Ceram. Int.* 45 (2019) 14015–14028. doi: 10.1016/j.ceramint.2019.04.101.
- [3] N. P. Wasekar, L. Bathini, L. Ramakrishna, D. S. Rao, and G. Padmanabham, Pulsed

- electrodeposition, mechanical properties and wear mechanism in Ni-W/SiC nanocomposite coatings used for automotive applications, *Appl. Surf. Sci.* 527 (2020) 146896. doi: 10.1016/j.apsusc.2020.146896.
- [4] M. Surender, R. Balasubramaniam, and B. Basu, Electrochemical behavior of electrodeposited Ni-WC composite coatings, *Surf. Coatings Technol.* 187 (2004) 93–97. doi: 10.1016/j.surfcoat.2004.01.030.
- [5] M. Qunshuang, L. Yajiang, and W. Juan, Effects of Ti addition on microstructure homogenization and wear resistance of wide-band laser clad Ni60/WC composite coatings, *Int. J. Refract. Met. Hard Mater.* 64 (2017) 225–233. doi: 10.1016/j.ijrmhm.2016.11.002.
- [6] M. Bedolla-Hernández, G. Rosano-Ortega, F. J. Sánchez-Ruiz, J. Bedolla-Hernández, P. S. Schabes-Retchkiman, and C. A. Vega-Lebrún, Electrodeposition mechanism of chromium nanoparticle coatings: Modeling and experimental validation, *Chem. Eng. Sci.* 252 (2022) 117291. doi: 10.1016/j.ces.2021.117291.
- [7] H. Hasannejad and T. Shahrabi, Economical deposition of Ni high cerium oxide nanocomposite coatings, *Surf. Eng.* 28 (2012) 418–423. doi: 10.1179/1743294411Y.0000000086.
- [8] Z. Zhang et al., Electrodeposition and wear behavior of NiCoW ternary alloy coatings reinforced by Al<sub>2</sub>O<sub>3</sub> nanoparticles: Influence of current density and electrolyte composition, *Surf. Coatings Technol.* 431 (2022) 128030. doi: 10.1016/j.surfcoat.2021.128030.
- [9] A. Chianpairot, G. Lothongkum, C. A. Schuh, and Y. Boonyongmaneerat, Corrosion of nanocrystalline Ni-W alloys in alkaline and acidic 3.5 wt.% NaCl solutions, *Corros. Sci.* 53 (2011) 1066–1071. doi: 10.1016/j.corsci.2010.12.001.
- [10] D. K. Singh and V. B. Singh, Electrodeposition and characterization of Ni-TiC composite using N-methylformamide bath, *Mater. Sci. Eng.* 532 (2012) 493–499. doi: 10.1016/j.msea.2011.10.115.
- [11] S. A. Lajevardi and T. Shahrabi, Effects of pulse electrodeposition parameters on the properties of Ni-TiO<sub>2</sub> nanocomposite coatings, *Appl. Surf. Sci.* 256 (2010) 6775–6781. doi: 10.1016/j.apsusc.2010.04.088.
- [12] A. Bigos et al., Citrate-based baths for electrodeposition of nanocrystalline nickel coatings with enhanced hardness, *J. Alloys Compd.* 850 (2021) 156857. doi: 10.1016/j.jallcom.2020.156857.
- [13] F. Ebrahimi and Z. Ahmed, The effect of current density on properties of electrodeposited nanocrystalline nickel. *J. Appl. Electrochem.* 33 (2003) 733–739. doi: 10.1023/A:1025049802635.
- [14] P. Gyftou, M. Stroumbouli, E. A. Pavlatou, and N. Spyrellis, Electrodeposition of Ni/SiC Composites by Pulse Electrolysis, *Trans. IMF.* 80 (2002) 88–91. doi: 10.1080/00202967.2002.11871440.
- [15] J. L. Stojak and J. B. Talbot, Investigation of Electrocodeposition Using a Rotating Cylinder Electrode, *J. Electrochem. Soc.* 146 (1999) 4504–4513. doi: 10.1149/1.1392665.
- [16] Y. Xuetao, W. Yu, S. Dongbai, and Y. Hongying, Influence of pulse parameters on the microstructure and microhardness of nickel electrodeposits, *Surf. Coatings Technol.* 202 (2008) 1895–1903. doi: 10.1016/j.surfcoat.2007.08.023.
- [17] M. E. Gamboa-Adelco and R. J. Gale, *A Guide to Problems in Modern Electrochemistry 1*. Boston, MA: Springer US, 2001. doi: 10.1007/978-1-4419-8600-9.
- [18] L. Venkatesh et al., Microstructure and phase evolution in laser clad chromium carbide-NiCrMoNb, *Appl. Surf. Sci.* 357 (2015) 2391–2401. doi: 10.1016/j.apsusc.2015.09.260.
- [19] S. Kamkar, M. Mohammadi and M. Karimi, Assessment of the Corrosion and Tribological Properties of Double Layer Nitride Coatings Performed by Plasma Nitriding and Cathodic Arc Evaporation on Ti-6Al-4V Alloy, 20 (2020) 1555–1565.
- [20] L. Zhang, X. Tang, Z. Wang, T. Li, Z. Zhang, and M. Lu, The Corrosion Behavior of 316L Stainless Steel in H<sub>2</sub>S environment at high temperatures, *Int. J. Electrochem. Sci.* 12 (2017) 8806–8819. doi: 10.20964/2017.09.17.
- [21] A. Günen, B. Soyulu, and Ö. Karakaş, Titanium carbide coating to improve surface characteristic, wear and corrosion resistance of spheroidal graphite cast



- irons, *Surf. Coatings Technol.* 437 (2022) 128280. doi: 10.1016/j.surfcoat.2022.128280.
- [22] X. Yang, X. Li, Q. Yang, H. Wei, X. Fu, and W. Li, Effects of WC on microstructure and corrosion resistance of directional structure Ni60 coatings, *Surf. Coatings Technol.* 385 (2020) 125359. doi: 10.1016/j.surfcoat.2020.125359.
- [23] F. F. Xia, W. C. Jia, C. Y. Ma, R. Yang, Y. Wang, and M. Potts, Synthesis and characterization of Ni-doped TiN thin films deposited by jet electrodeposition, *Appl. Surf. Sci.* 434 (2018) 228–233. doi: 10.1016/j.apsusc.2017.10.203.
- [24] N. Dai, L. C. Zhang, J. Zhang, Q. Chen, and M. Wu, Corrosion behavior of selective laser melted Ti-6Al-4 V alloy in NaCl solution, *Corros. Sci.* 102 (2016) 484–489. doi: 10.1016/j.corsci.2015.10.041.
- [25] J. D. Voorhies, Electrochemical and Chemical Corrosion of Tungsten Carbide (WC), *J. Electrochem. Soc.* 119 (1972) 219. doi: 10.1149/1.2404164.
- [26] W. Wang, L. Qian, Y. Zhang, and Y. Zhang, Electrochemical impedance spectroscopy characteristics of steel corrosion in seawater sea-sand concrete, *IOP Conf. Ser. Earth Environ. Sci.* 267 (2019) 042017. doi: 10.1088/1755-1315/267/4/042017.
- [27] M. Saremi and M. Yeganeh, Corrosion behavior of copper thin films deposited by EB-PVD technique on thermally grown silicon dioxide and glass in hydrochloric acid media, *Mater. Chem. Phys.* 123 (2010) 456–462. doi: 10.1016/j.matchemphys.2010.04.041.
- [28] S.A. Naziri Mehrabani, R. Ahmadzadeh, N. Abdian, A. Taghizadeh Tabrizi, and H. Aghajani, Synthesis of Ni-GO nanocomposite coatings: Corrosion evaluation, *Surf. Interfaces.* 20 (2020) 100546. Doi: org/10.1016/j.surf.2020.100546.
- [29] N. Guglielmi, Kinetics of the Deposition of Inert Particles from Electrolytic Baths, *J. Electrochem. Soc.* 119 (1972) 1009-1012. doi 10.1149/1.2404383.